arXiv:0909.1380v1 [hep-ph] 8 Sep 2009

Further evidence for the Σ^* resonance with $J^P = 1/2^-$ around 1380 MeV

Jia-Jun Wu[1], S. Dulat[2,3] and B. S. Zou[1,3]

[1] Institute of High Energy Physics, CAS, P.O.Box 918(4), Beijing 100049, China

[2] School of Physics Science and Technology, Xinjiang University, Urumqi, 830046, China

[3] Theoretical Physics Center for Science Facilities, CAS, Beijing 100049, China

(Dated: September 7, 2009)

Abstract

The unquenched quark models predict the new particle Σ^* with spin parity $J^P = 1/2^-$ and its mass is around the well established $\Sigma^*(1385)$ with $J^P = 3/2^+$. Here by using the effective Lagrangian approach we study $K^- p \to \Lambda\pi^-\pi^+$ reaction at the range of $\Lambda^*(1520)$ peak, comparing the resulting total cross section, and $\pi^+\pi^-$, $\Lambda\pi^+$, $\Lambda\pi^-$ invariant squared mass distributions for various incident K^- momenta, as well as the production angular distribution of the Λ with the data from the Lawrence Berkeley Laboratory 25-inch hydrogen bubble chamber, we find that, apart from the existing resonance $\Sigma^*(1385)$ with $J^P = 3/2^+$, there is a strong evidence for the existence of the new resonance Σ^* with $J^P = 1/2^-$ around 1380 MeV. Higher statistic data on relevant reactions are needed to clarify the situation.

I. INTRODUCTION

The classical constituent quark models are based on the assumption of three constituent quarks inside each baryon. They are very successful for the spatial ground state of baryons, but have serious problems for the predictions of baryon excitation states. The lowest excitation of baryons is expected to be the orbital angular momentum $L = 1$ excitation of a quark, resulting to spin-parity $1/2^-$. The $N^*(1535)$, $\Lambda^*(1405)$ and $\Sigma^*(1620)$ are the lowest $1/2^-$ baryons from many experiments [1]. There is a question that why the mass of $\Lambda^*(1405)$ is much less than $N^*(1535)$. It is very difficult to explain this problem in the classical 3-quark models, because the $\Lambda^*(1405)$ with (uds)-quarks is obviously expected to be heavier than $N^*(1535)$ with (uud)-quarks. Another problem is about the $\bar{d}/\bar{u}$ asymmetry in the proton with the number of $\bar{d}$ more than $\bar{u}$ by an amount $\bar{d} - \bar{u} \approx 0.12$ [2]. If one wants to solve these problems, one should put the $q\bar{q}$ components in the baryons. The unquenched models give the good explanation to these problems. For example, in the penta-quark models [3, 4, 5], the mass of $N^*(1535)$ with mainly a $[ud][us]\bar{s}$ state is heavier than $\Lambda^*(1405)$ with mainly a $[ud][sq]\bar{q}$ state with $q\bar{q} = (u\bar{u} + d\bar{d})/\sqrt{2}$. The 5-quark models may play an important role in the baryon spectroscopy.

These unquenched models give many new predictions besides the properties of $\Lambda^*(1405)$ and $N^*(1535)$. In fact, the penta-quark models [3, 4] show a new physical picture for the baryonic excitation. The lowest excitation is $J^P = 1/2^-$ in the $qqqq\bar{q}$ model, and there are two new particles $\Sigma^*(1360 - 1405)$ and $\Xi^*(1520)$ which are absent in the qqq model. The meson cloud model [6] predicts them to be non-resonant broad structures. These new predictions are all very different from the results of the classical quenched quark models, so it needs to be checked by experiments.

Possible existence of such new $\Sigma^*(1/2^-)$ structure in J/ψ decays was pointed out earlier [7] and is going to be investigated by the starting BES3 experiment [8], and we also re-examined the old data of $K^- p \to \Lambda\pi^+\pi^-$ reaction at $Plab_{(K^-)} = 1.0 - 1.8$ GeV to find some evidence for its existence [9]. In this paper by using the results from the fit of experimental data in the Ref. [9], we show further evidence for the existence of such $\Sigma^*(1/2^-)$ in the $K^- p \to \Lambda^*(1520) \to \Sigma^*\pi \to \Lambda\pi^+\pi^-$ reaction at $Plab_{(K^-)} = 0.25 - 0.60$ GeV, with a very clear peak of $\Lambda^*(1520)$ in the energy dependence of the total cross section [10, 11].

In the next section, we present the formalism and ingredients for the study of the $K^- p \to$

$\Lambda\pi^-\pi^+$ reaction by including various Feynman diagrams. In the last section, our numerical results, comparision with the experimental data, and conclusions are given.

II. FORMALISM AND INGREDIENTS

In this section we present the formalism and ingredients for the analysis of

$$K^- p \to \Lambda\pi^-\pi^+ \tag{1}$$

in the energy region around the $\Lambda^*(1520)$. First, the corresponding Feynman diagrams, s-channel $\Lambda^\star(1520)$ exchange diagram (a), u-channel n exchange diagram (b), t-channel K^{*0} exchange diagram (c), t-channel K^{*0} and n exchange diagram (d), t-channel K^{*0} and K^- exchange diagram (e), and u-channel n and p exchange diagram (f), for the reaction (1) are depicted in Fig. 1.

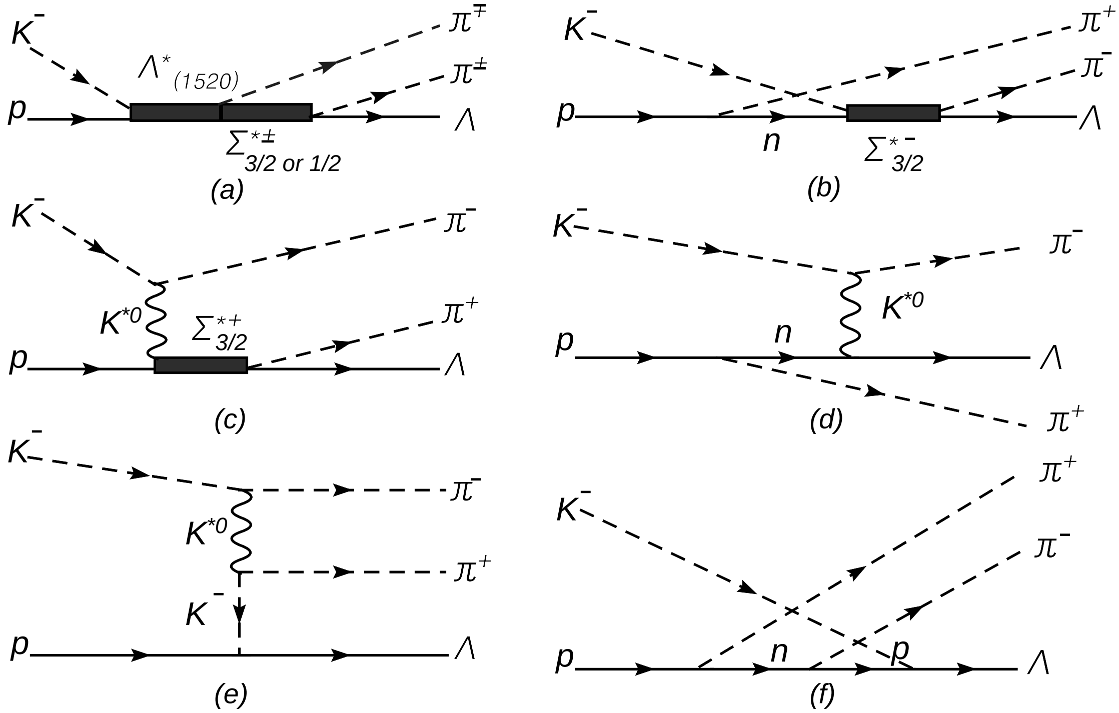

FIG. 1: The Feynman diagrams of the $K^- p \to \Lambda\pi^-\pi^+$ reaction.

Besides we give the effective Lagrangian densities for describing the interaction vertices in Fig. 1. They can be written as

$$\mathcal{L}_{\Lambda^* KN} = g_{\Lambda^* KN}\bar{\Lambda}^{*\nu}\gamma_5\gamma^\mu N\partial_\nu\partial_\mu\bar{K} + h.c., \tag{2}$$

$$\mathcal{L}_{\Lambda^*\Sigma^*_{3/2}\pi} = g_{\Lambda^*\Sigma^*_{3/2}\pi}\bar{\Lambda}^*_\mu\Sigma^{*\mu}_{3/2}\pi + h.c., \tag{3}$$

$$\mathcal{L}_{\Sigma^*_{3/2}\Lambda\pi} = g_{\Sigma^*_{3/2}\Lambda\pi}\bar{\Lambda}\Sigma^{*\mu}_{3/2}\partial_\mu\pi + h.c., \tag{4}$$

$$\mathcal{L}_{\Lambda^*\Sigma^*_{1/2}\pi} = g_{\Lambda^*\Sigma^*_{1/2}\pi}\bar{\Lambda}^*_\mu\Sigma^*_{1/2}\partial^\mu\vec{\pi}\cdot\vec{\tau} + h.c., \tag{5}$$

$$\mathcal{L}_{\Sigma^*_{1/2}\Lambda\pi} = g_{\Sigma^*_{1/2}\Lambda\pi}\bar{\Lambda}\Sigma^*_{1/2}\vec{\pi}\cdot\vec{\tau} + h.c., \tag{6}$$

$$\mathcal{L}_{\Sigma^*_{3/2}KN} = \frac{g_{\Sigma^*_{3/2}KN}}{m_K}\bar{\vec{\Sigma}}^*_{3/2\mu}\cdot\vec{\tau}N\partial^\mu\bar{K} + h.c., \tag{7}$$

$$\mathcal{L}_{NN\pi} = \frac{g_{NN\pi}}{2m_N}\bar{N}\gamma_5\gamma_\mu N\partial^\mu\vec{\pi}\cdot\vec{\tau} + h.c., \tag{8}$$

$$\mathcal{L}_{K^*K\pi} = g_{K^*K\pi}K^{*\mu}(\vec{\pi}\cdot\vec{\tau}\partial_\mu K - K\partial_\mu\vec{\pi}\cdot\vec{\tau}) + h.c., \tag{9}$$

$$\mathcal{L}_{\Sigma^*_{3/2}K^*N} = \frac{g_{\Sigma^*_{3/2}K^*N}}{2m_N}\bar{\vec{\Sigma}}^*_{3/2\mu}\cdot\vec{\tau}\gamma_\nu\gamma_5 N(\partial^\nu\bar{K}^{*\mu} - \partial^\mu\bar{K}^{*\nu}) + h.c., \tag{10}$$

$$\mathcal{L}_{\Lambda K^*N} = \bar{\Lambda}(g_{\Lambda K^*N}\gamma_\mu + \frac{f_{\Lambda K^*N}}{2m_\Lambda}\sigma_{\mu\nu}\partial^\nu)\bar{K}^{*\mu}N + h.c., \tag{11}$$

$$\mathcal{L}_{\Lambda KN} = \frac{g_{\Lambda KN}}{2m_\Lambda}\bar{\Lambda}\gamma_5\gamma_\mu N\partial^\mu\bar{K} + h.c.. \tag{12}$$

Here m_K, m_N and m_Λ are the kaon, nucleon and Λ masses; $\Sigma^*_{3/2\mu}$ and Λ^*_μ are Rarita-Schwinger fields for $\Sigma^*(1385)$ and $\Lambda^*(1520)$ of spin-3/2 particles; $\Sigma^*_{1/2}$, N and Λ are the spin-half fields for the $\Sigma^*(1380)$, N(938) and $\Lambda(1115)$ particles; π and K are scalar fields for the pion and kaon; $\vec{\tau}$ is a usual isospin-1/2 Pauli matrix operator; the relevant interaction coupling constants, obtained by using the above effective Lagrangians to fit relevant decay widths or from literature, are all listed in Table I.

Furthermore, we need also the propagators of resonant particles to calculate Feynman diagrams. For the K and K^* mesons, the propagators are:

$$G_{K(q)} = \frac{1}{q^2 - m_K^2}, \tag{13}$$

$$G_{K^*(q)} = \frac{-g_{\mu\nu} + q^\mu q^\nu/m^2_{K^*}}{q^2 - m^2_{K^*} + i\Gamma_{K^*}m_{K^*}}. \tag{14}$$

For the spin-1/2 and spin-3/2 baryon resonances the propagators can be written as [12]:

$$G^{\frac{1}{2}}_{R(q)} = \frac{(\not{p} + m)}{q^2 - m_R^2 + im_R\Gamma_R}, \tag{15}$$

$$G^{\frac{3}{2}}_{R(q)} = \frac{(\not{p} + m)}{q^2 - m_R^2 + im_R\Gamma_R}\left(-g_{\mu\nu} + \frac{1}{3}\gamma_\mu\gamma_\nu + \frac{2}{3}\frac{q_\mu q_\nu}{m_R^2} + \frac{1}{3m_R}(\gamma_\mu q_\nu - \gamma_\nu q_\mu)\right). \tag{16}$$

R	$\Gamma_R(GeV)$	Decay mode	Branching ratios	$g^2/4\pi(f^2/4\pi)$
$\Lambda^*(1520)$	0.0156	NK	0.45	11.88
		$\Sigma\pi$	0.42	7.38
		$\Sigma^*_{3/2}\pi \to \Lambda\pi\pi$	0.11 [11]	0.56 (a)
		$\Sigma^*_{1/2}\pi \to \Lambda\pi\pi$	0.11 [11]	3.57 (b)
K^*	0.0508	$K\pi$	0.9976	2.52
$\Sigma^*_{3/2}$	0.0358	$\Lambda\pi$	0.87	6.68
		K^*N		2.39 [13]
		KN		0.83 [13]
Λ		K^*N		1.588 (5.175) [14]
		KN		3.506 [14]
N		$N\pi$		14.4 [12]

TABLE I: Parameters used in our calculation. Widths and branching ratios are from PDG [1]; the mass and width of $\Sigma^*_{1/2}$ are 1.3813 GeV and 0.1186 GeV, respectively [9]; for (a) and (b) we use $(g_{\Lambda^*\Sigma^*\pi}g_{\Sigma^*\Lambda\pi})^2/(4\pi)^2$, while assuming that all $\Lambda\pi\pi$ come from $\Sigma^*\pi$ in the $\Lambda^* \to \Lambda\pi\pi$ reaction.

The role of $\Lambda^*(1520)$ is very important, thus we take into account that the width $\Gamma_{\Lambda^*(1520)}$ of the $\Lambda^*(1520)$ is dependent on its four-momentum squared, and by straightforward calculation we obtain the following expression for the $\Gamma_{\Lambda^*(1520)}$

$$\Gamma_{\Lambda^*(1520)(s)} = \Gamma_{\Lambda^*NK(s)} + \Gamma_{\Lambda^*\Sigma\pi(s)} + \Gamma_{\Lambda^*\Lambda\pi\pi(s)} + \Gamma_0, \tag{17}$$

where

$$\begin{aligned}
\Gamma_{\Lambda^*NK(s)} &= \frac{g^2_{\Lambda^*NK}}{4\pi}\frac{|\vec{p}_{K(s)}|^3(2\sqrt{s}|\vec{p}_{K(s)}|^2 + m_K^2(\sqrt{m_N^2+|\vec{p}_{K(s)}|^2} - m_p))}{3\sqrt{s}}, && (18)\\
\Gamma_{\Lambda^*\Sigma\pi(s)} &= \frac{g^2_{\Lambda^*\Sigma\pi}}{4\pi}\frac{|\vec{p}_{\pi(s)}|^3(2\sqrt{s}|\vec{p}_{\pi(s)}|^2 + m_\pi^2(\sqrt{m_\Sigma^2+|\vec{p}_{\pi(s)}|^2} - m_\Sigma))}{3\sqrt{s}}, && (19)\\
\Gamma_{\Lambda^*\Lambda\pi\pi(s)} &= \Gamma_{\Lambda^*\to\Sigma^*_{3/2}\pi\to\Lambda\pi\pi(s)} \times R_{3/2} + \Gamma_{\Lambda^*\to\Sigma^*_{1/2}\pi\to\Lambda\pi\pi(s)} \times (1-R_{3/2}), && (20)\\
\Gamma_0 &= 0.4MeV \quad for\ \ \Gamma_{\Lambda^*_{1520}(\sqrt{s}=1.5196GeV)} = 15.6MeV && (21)
\end{aligned}$$

and where

$$\begin{aligned}
|\vec{p}_{K(s)}| &= \frac{\sqrt{s}}{2}\sqrt{(1-\frac{(m_K+m_N)^2}{s})(1-\frac{(m_K-m_N)^2}{s})}\,, && (22)\\
|\vec{p}_{\pi(s)}| &= \frac{\sqrt{s}}{2}\sqrt{(1-\frac{(m_\pi+m_\Sigma)^2}{s})(1-\frac{(m_\pi-m_\Sigma)^2}{s})} && (23)
\end{aligned}$$

are the magnitudes of the three momenta of the K and π mesons;

$$\begin{aligned}\Gamma_{\Lambda^*\to\Sigma^*_{3/2}\pi\to\Lambda\pi\pi(s)} &= \int |M_{\Lambda^*\to\Sigma^*_{3/2}\pi\to\Lambda\pi\pi(s)} B1_{(Q_{\Sigma^*_{3/2}\Lambda\pi})} F_{\Sigma^*_{3/2}}|^2 d\phi_{\Lambda^*\to\Lambda\pi\pi}, &(24)\\ \Gamma_{\Lambda^*\to\Sigma^*_{3/2}\pi\to\Lambda\pi\pi(s)} &= \int |M_{\Lambda^*\to\Sigma^*_{1/2}\pi\to\Lambda\pi\pi(s)} B1_{(Q_{\Lambda^*\Sigma^*_{1/2}\pi})} F_{\Sigma^*_{1/2}}|^2 d\phi_{\Lambda^*\to\Lambda\pi\pi}, &(25)\end{aligned}$$

are the decay widths for the processes $\Lambda^* \to \Sigma^*_{3/2}\pi \to \Lambda\pi\pi$ and $\Lambda^* \to \Sigma^*_{1/2}\pi \to \Lambda\pi\pi$, respectively. Here $M_{\Lambda^*\to\Sigma^*_{3/2}\pi\to\Lambda\pi\pi(s)}$ and $M_{\Lambda^*\to\Sigma^*_{1/2}\pi\to\Lambda\pi\pi(s)}$ are the corresponding amplitudes; $\phi_{\Lambda^*\to\Lambda\pi\pi}$ is the phase space of Λ^* decays into $\Lambda\pi\pi$; the form factor F_R and Blatt-Weisskopf centrifugal barrier factor $B1_{(Q_{abc})}$ are given in Eqs.(26) and (27), respectively; the parameter $R_{3/2}$ stands for the proportion of $\Sigma^*_{3/2}$ in the Σ^*.

Since the baryons and mesons are not point-like particles we need to consider the form factors for each interaction vertices in order to calculate amplitudes for the reaction. Therefore now we give the form factors for every Feynman diagram. For the Fig.1(a), we use the following form factors

$$F_R(q^2) = \frac{\Lambda^4}{\Lambda^4 + (q^2 - m_R^2)^2} \qquad (26)$$

with $\Lambda = 0.8GeV$ ($R = \Lambda^*$ or Σ^*) [12]. Because both the Λ^* and Σ^* are almost on-shell, the contribution of these form factors are unimportant. In addition, we also use the following P-wave and D-wave Blatt-Weisskopf barrier form factors for the vertices of $\Lambda^*\Sigma^*_{1/2}\pi$, $\Sigma^*_{3/2}\Lambda\pi$ and $\Lambda^* NK$

$$\begin{aligned}B1_{(Q_{abc})} &= \sqrt{\frac{\tilde{Q}^2_{abc} + Q_0^2}{Q^2_{abc} + Q_0^2}}, &(27)\\ B2_{(Q_{abc})} &= \sqrt{\frac{\tilde{Q}^4_{abc} + 3\tilde{Q}^2_{abc}Q_0^2 + 9Q_0^4}{Q^4_{abc} + 3Q^2_{abc}Q_0^2 + 9Q_0^4}}, &(28)\end{aligned}$$

with

$$\begin{aligned}Q^2_{abc} &= \frac{(s_a + s_b - s_c)^2}{4s_a} - s_b, &(29)\\ \tilde{Q}^2_{abc} &= \frac{(m_a^2 + m_b^2 - m_c^2)^2}{4m_a^2} - m_b^2. &(30)\end{aligned}$$

Here $Q_0 = 0.197321/R$ is a hadron scale parameter in the unit of GeV/c with R the radius of the centrifugal barrier in the unit of fm. In our calculation we set $R = 0.2fm$. We find that these two form factors have negligible effect on our results, thus one may conclude that Fig.1(a) is almost model independent.

For the Figs.1(b,c), we use Eq.(27) for the $\Sigma^*_{3/2}\Lambda\pi$ vertex, and Eq.(26) for the off-shell baryon resonance $\Sigma^*_{3/2}$ with cut-off parameter $\Lambda = 1.0$ GeV for K^* exchange and n exchange.

For the Figs.1(d,e,f), we also use the form factor in Eq.(26) with $\Lambda = 1.0$ GeV for K^* and K^- exchange diagram, and $\Lambda = 1.8$ GeV for n and p exchange diagram.

After fixing the relevant effective Lagrangians, coupling constants, propagators and form factors, the amplitudes for various Feynman diagrams can be written down straightforwardly by following the Feynman rules, and total amplitude is just their simple sum. Here as an example, we give explicitly the individual amplitudes corresponding to $\Lambda^* \to \Sigma^*_{3/2}\pi$ and to $\Lambda^* \to \Sigma^*_{1/2}\pi$ for the Feynman diagrams (a) in the Fig.1,

$$\begin{aligned}
\mathcal{M}_{\Lambda^*\to\Sigma^*_{3/2}\pi} &= \mathcal{M}_{\Lambda^*\to\Sigma^{*+}_{3/2}\pi^-} + \mathcal{M}_{\Lambda^*\to\Sigma^{*-}_{3/2}\pi^+} \\
&= \frac{g_{\Lambda^*KN}\, g_{\Lambda^*\Sigma^*_{3/2}\pi}\, g_{\Sigma^*_{3/2}\Lambda\pi}}{\sqrt{6}} F_{\Lambda^*} B2_{(Q_{\Lambda^*NK})} \bar{u}_{p_\Lambda s_\Lambda} \Big(p^\alpha_{\pi^+} G^{(\frac{3}{2})}_{\Sigma^{*+}_{3/2}\alpha\mu} F_{\Sigma^{*+}_{3/2}} B1_{(Q_{\Sigma^{*+}_{3/2}\Lambda\pi^+})} \\
&\quad + p^\alpha_{\pi^-} G^{(\frac{3}{2})}_{\Sigma^{*-}_{3/2}\alpha\mu} F_{\Sigma^{*-}_{3/2}} B1_{(Q_{\Sigma^{*-}_{3/2}\Lambda\pi^-})} \Big) G^{(\frac{3}{2})\mu\nu}_{\Lambda^*} p_{K^-\nu} \gamma_5 \not{p}_{K^-} u_{p_p s_p}, \qquad (31) \\
\mathcal{M}_{\Lambda^*\to\Sigma^*_{1/2}\pi} &= \mathcal{M}_{\Lambda^*\to\Sigma^{*+}_{1/2}\pi^-} + \mathcal{M}_{\Lambda^*\to\Sigma^{*-}_{1/2}\pi^+} \\
&= \frac{g_{\Lambda^*KN}\, g_{\Lambda^*\Sigma^*_{1/2}\pi}\, g_{\Sigma^*_{1/2}\Lambda\pi}}{\sqrt{6}} F_{\Lambda^*} B2_{(Q_{\Lambda^*NK})} \bar{u}_{p_\Lambda s_\Lambda} \Big(G^{(\frac{1}{2})}_{\Sigma^{*+}_{1/2}} p_{\pi^-\mu} F_{\Sigma^{*+}_{1/2}} B1_{(Q_{\Lambda^*\Sigma^{*+}_{1/2}\pi^-})} \\
&\quad + G^{(\frac{1}{2})}_{\Sigma^{*-}_{1/2}} p_{\pi^+\mu} F_{\Sigma^{*-}_{1/2}} B1_{(Q_{\Lambda^*\Sigma^{*-}_{1/2}\pi^+})} \Big) G^{(\frac{3}{2})\mu\nu}_{\Lambda^*} p_{K^-\nu} \gamma_5 \not{p}_{K^-} u_{p_p s_p}, \qquad (32)
\end{aligned}$$

where $u_{p_\Lambda s_\Lambda}$ and $u_{p_p s_p}$ are the spin wave functions of the outgoing Λ and incoming proton, respectively; p_{π^+}, p_{π^-} and p_{K^-} are the 4- momenta of the final state pions and initial state K^- meson; the factor $1/\sqrt{6}$ is a isospin C-G coefficient. So the total amplitude squared for the $K^-p \to \Lambda\pi^-\pi^+$ reaction is

$$\begin{aligned}
|\mathcal{M}_{K^-p\to\Lambda\pi^+\pi^-}|^2 &= |\mathcal{M}_{\Lambda^*\to\Sigma^*_{3/2}\pi}|^2 \times R_{3/2} + |\mathcal{M}_{\Lambda^*\to\Sigma^*_{1/2}\pi}|^2 \times (1 - R_{3/2}) + \\
&\quad |\mathcal{M}_{n\Sigma^{*-}_{3/2}\pi^+}|^2 + |\mathcal{M}_{K^{*0}\Sigma^{*-}_{3/2}\pi^+}|^2 + \\
&\quad |\mathcal{M}_{K^{*0}n}|^2 + |\mathcal{M}_{K^{*0}K^-}|^2 + |\mathcal{M}_{pn}|^2. \qquad (33)
\end{aligned}$$

Note that we do not include the interference terms between different Feynman diagrams because their contributions are insignificant. Then the calculation of the cross section for $K^-p \to \Lambda\pi^-\pi^+$ is straightforward:

$$\begin{aligned}
d\sigma_{K^-p\to\Lambda\pi^+\pi^-} &= \frac{1}{4} \frac{m_p}{\sqrt{(p_p \cdot p_{K^-})^2 - m_p m_{K^-}}} \sum_{s_i} \sum_{s_f} |\mathcal{M}_{K^-p\to\Lambda\pi^+\pi^-}|^2 d\phi, \qquad (34) \\
d\phi &= \frac{1}{(2\pi)^5} \frac{m_\Lambda d^3p_\Lambda}{E_\Lambda} \frac{d^3p_{\pi^+}}{2E_{\pi^+}} \frac{d^3p_{\pi^-}}{2E_{\pi^-}} \delta^4(p_{K^-} + p_p - p_\Lambda - p_{\pi^+} - p_{\pi^-}). \qquad (35)
\end{aligned}$$

III. NUMERICAL RESULTS AND DISCUSSION

With the formalism and ingredients given in the former section, we compute the total cross section versus the K^- beam momentum $Plab_{(K^-)}$ for the $K^-p \rightarrow \Lambda\pi^-\pi^+$ reaction for $Plab_{(K^-)} = 0.25 - 0.60$ GeV by using the code FOWL from the CERN program library, which is a program for Monte Carlo multi-particle phase space integration weighted by the amplitude squared. We consider two cases, firstly, we assume that the J^P of the Σ^* is $\frac{3}{2}^+$ with $R_{3/2} = 1.0$. On the other hand, we suppose that the Σ^* with $J^P = \frac{3}{2}^+$ and with $J^P = \frac{1}{2}^-$ account for 60% and 40%, respectively ($R_{3/2} = 0.60$). Our results on the total cross section for the $K^-p \rightarrow \Lambda\pi^-\pi^+$ reaction is almost the same for both cases, because the branching ratio of $\Lambda^*(1520) \rightarrow \Lambda\pi\pi$ is 11% for both cases. Total cross section, angular distributions of the final state Λ, and $\pi\pi$, $\Lambda\pi^+$, $\Lambda\pi^-$ invariant mass square distributions, as well as Dalitz plots for the final state particles for the two cases of our theoretical calculations, are shown in Figs.2-7, with experimental data points from the Refs.[11, 16, 17].

Comparison with the experimental data in Refs.[11, 16, 17] for the total cross section of $K^-p \rightarrow \Lambda\pi^-\pi^+$ in Fig.2 shows that for the energies below 0.355GeV our theoretical calculation result does not fit well with experiment. The reason may be the absence of the contribution of $\Lambda^*(1405)$ or other resonance states. For the energies larger than 0.42 GeV, the contribution of Feynman diagram Fig.1(b) becomes large, but the contribution is uncertain because of the large influence of form factor. Further detailed study is necessary for this energy range. For the energies from 0.355 to 0.42 GeV, the theoretical prediction agrees very well with the experiment, and the main contribution comes from the decay $\Lambda^*(1520) \rightarrow \Sigma^{*\pm}\pi^{\mp}$. Therefore the decay $\Lambda^*(1520) \rightarrow \Sigma^{*\pm}\pi^{\mp}$ is the interesting place to search for the evidence of $\Sigma^*_{1/2}$.

The theoretical angular distributions in Fig.3 of the Λ are almost the same for the pure $\Sigma^*(1385)$ with $J^P = \frac{3}{2}^+$ and for the 60% $\Sigma^*(1385)$ plus 40% $\Sigma^*_{1/2-}$ ($R_{3/2} = 0.60$).

There are quite large differences between the two theoretical invariant mass squared distributions which are shown in Figs.4, 5, 6, especially the invariant mass squared spectra of $\Lambda\pi$. One may note that the solid curves with both $\Sigma^*_{3/2}$ and $\Sigma^*_{1/2}$ contributions give much better agreement with the experiment data.

To understand the reason for the difference, we show the Dalitz plots for the two reaction

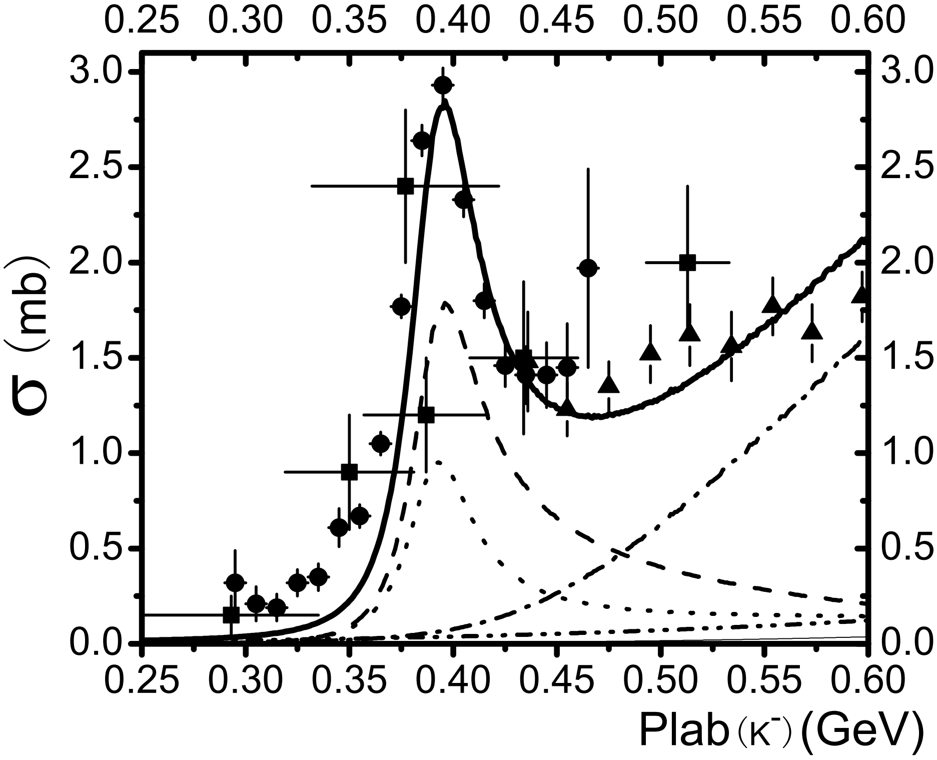

FIG. 2: Theoretical total cross section vs beam momentum $Plab_{(K^-)}$ for the $K^-p \to \Lambda\pi^+\pi^-$ reaction with $R_{3/2} = 0.60$. The circle, square and triangle are data points from [11], [16] and [17], respectively. The dashed and dotted curves are for the Fig.1(a) with $\Sigma^*_{3/2}$ and $\Sigma^*_{1/2}$, respectively; the dash-dotted and the dash-dot-dotted curves for the Fig.1(b) and Fig.1(d), respectively; curves close to zero for Fig.1(c,e,f). The solid curve is the sum of these broken curves.

sequences

$$K^-p \to \Lambda^* \to \Sigma^{*-}_{3/2}\pi^+ \to \Lambda\pi^+\pi^- \tag{36}$$

$$K^-p \to \Lambda^* \to \Sigma^{*-}_{1/2}\pi^+ \to \Lambda\pi^+\pi^- \tag{37}$$

at $Plab_{(K^-)} = 0.394GeV$ in Fig.7. From Fig.7 (a) and (b) we see that, the contribution of (36) is distributed on the top left corner, but of (37) is in the middle. This is because for the decay $\Lambda^* \to \Sigma^{*-}_{3/2}\pi^+$, the final state particles are in the relative S-wave, while for the decay $\Lambda^* \to \Sigma^{*-}_{1/2}\pi^+$, they are in the relative P-wave with large $\Sigma^{*-}_{1/2}$ width. From these Dalitz

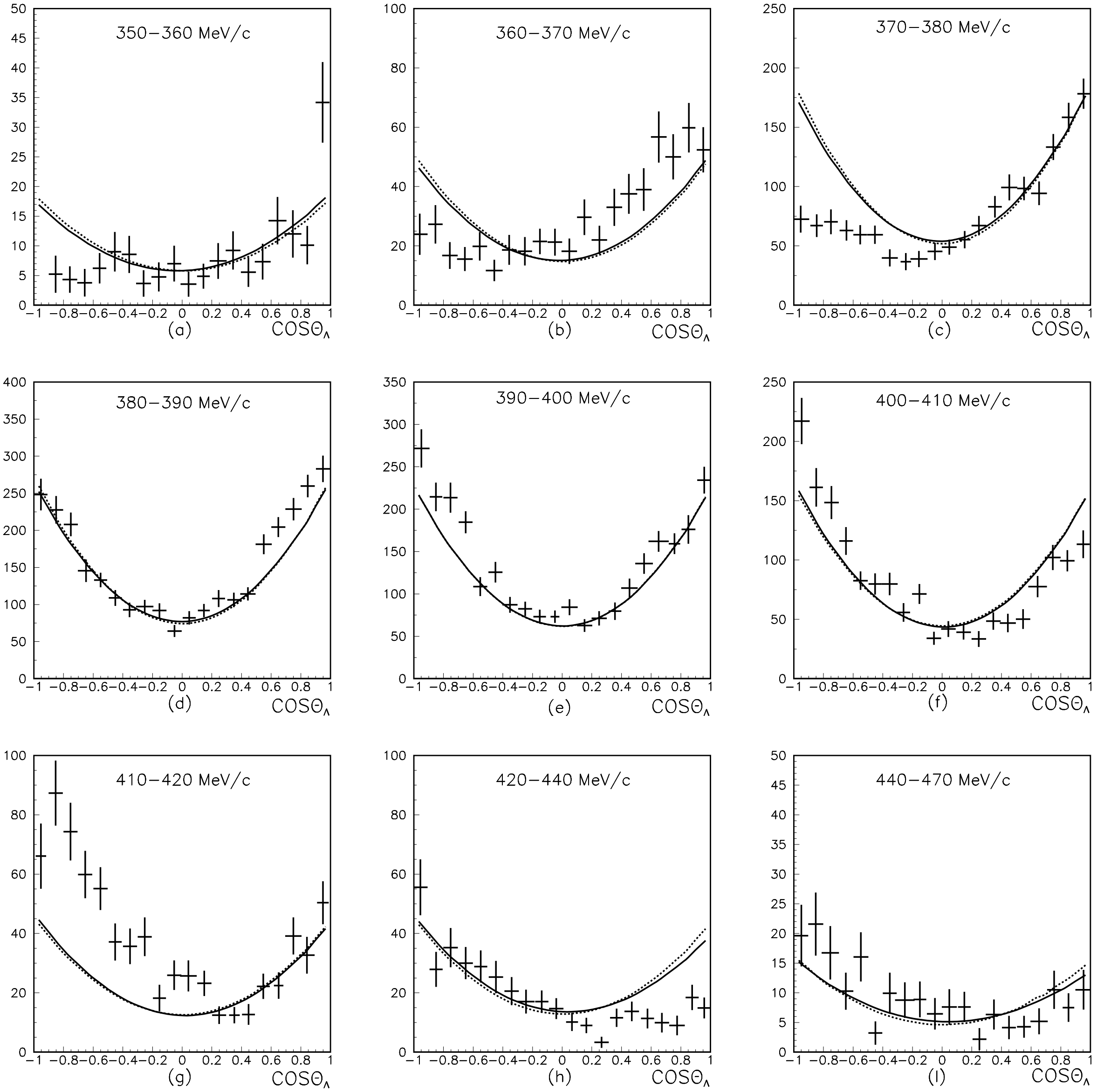

FIG. 3: Theoretical angular distribution of the Λ for various K^- beam momenta compared with data [11]. The dotted line is for the pure $\Sigma^*(1385)$ with $J^P = \frac{3}{2}^+$; the solid line includes $\Sigma^*_{1/2}$ in addition with $R_{3/2} = 0.60$.

plots, one can understand why there is so much difference in the invariant mass squared spectra of $\Lambda\pi$. The experimental analysis in Ref.[11] also considered the contribution of the S-wave of $\Lambda\pi$, which may come from $\Sigma^*_{1/2}$, also the $\pi^+\pi^-$ from the σ or ρ, but the range of invariance mass spectrum of $\pi^+\pi^-$ is from 0.28 to 0.4 GeV, which is far from the mass of σ or ρ. By the investigation we also find that the S-wave final state interaction (FSI) of $\pi^+\pi^-$

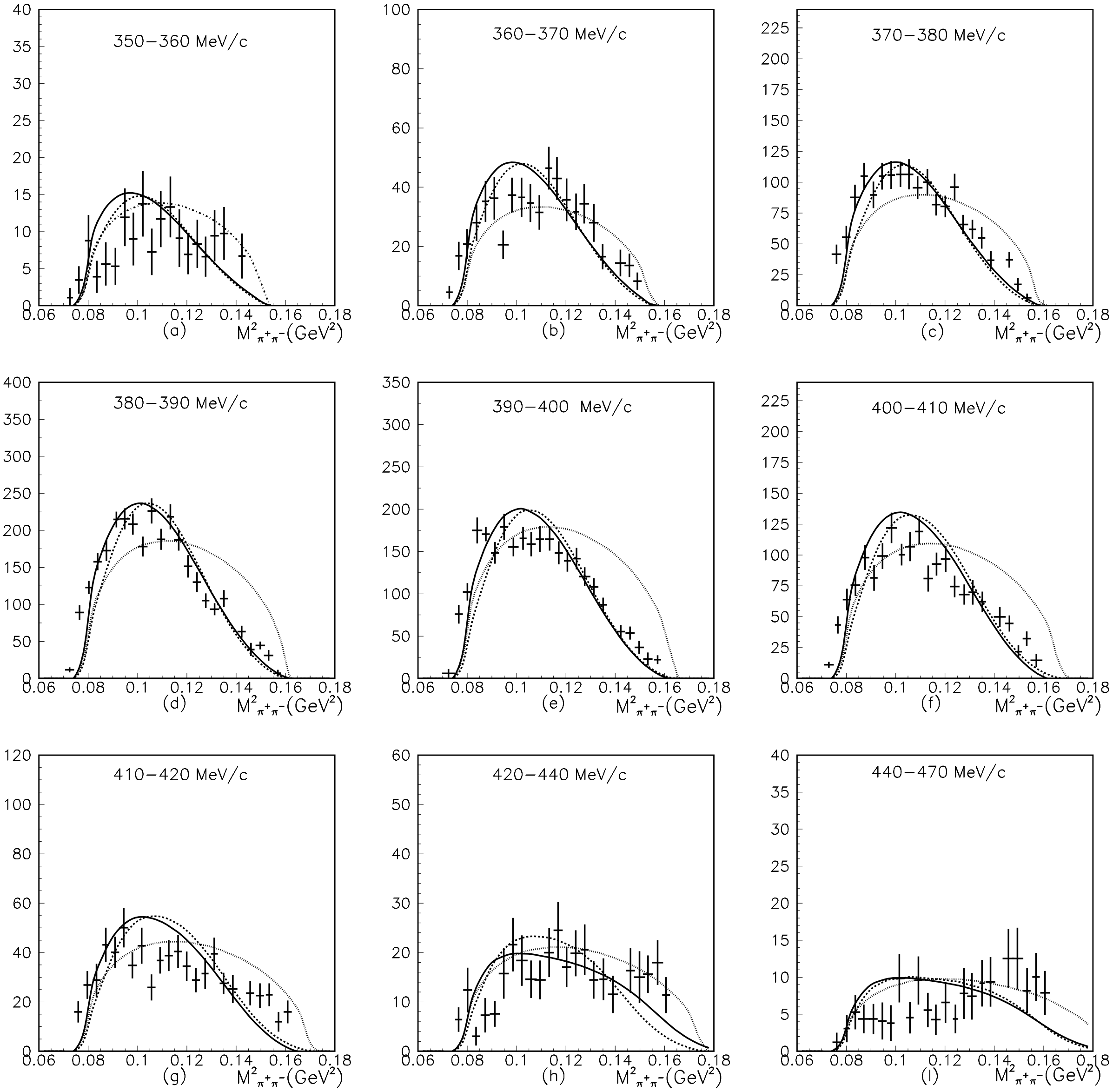

FIG. 4: Theoretical $\pi^+\pi^-$ invariant mass squared distribution for various K^- beam momenta compared with data [11]. The dotted line is for the pure $\Sigma^*(1385)$ with $J^P = \frac{3}{2}^+$; the solid line includes $\Sigma^*_{1/2}$ in addition with $R_{3/2} = 0.60$.

has little influence on the $\Lambda\pi$ invariant mass squared spectra. Thus we conclude that there should be contribution from the $\Sigma^*_{1/2}$ for the reaction at energies around the $\Lambda^*(1520)$ peak. For the $\pi^+\pi^-$ invariance mass spectra, the inclusion of 40% $\Sigma^*_{1/2}$ gives some enhancement to the low energy end and reproduces better the data for Kp center of mass energies around the $\Lambda^*(1520)$ peak.

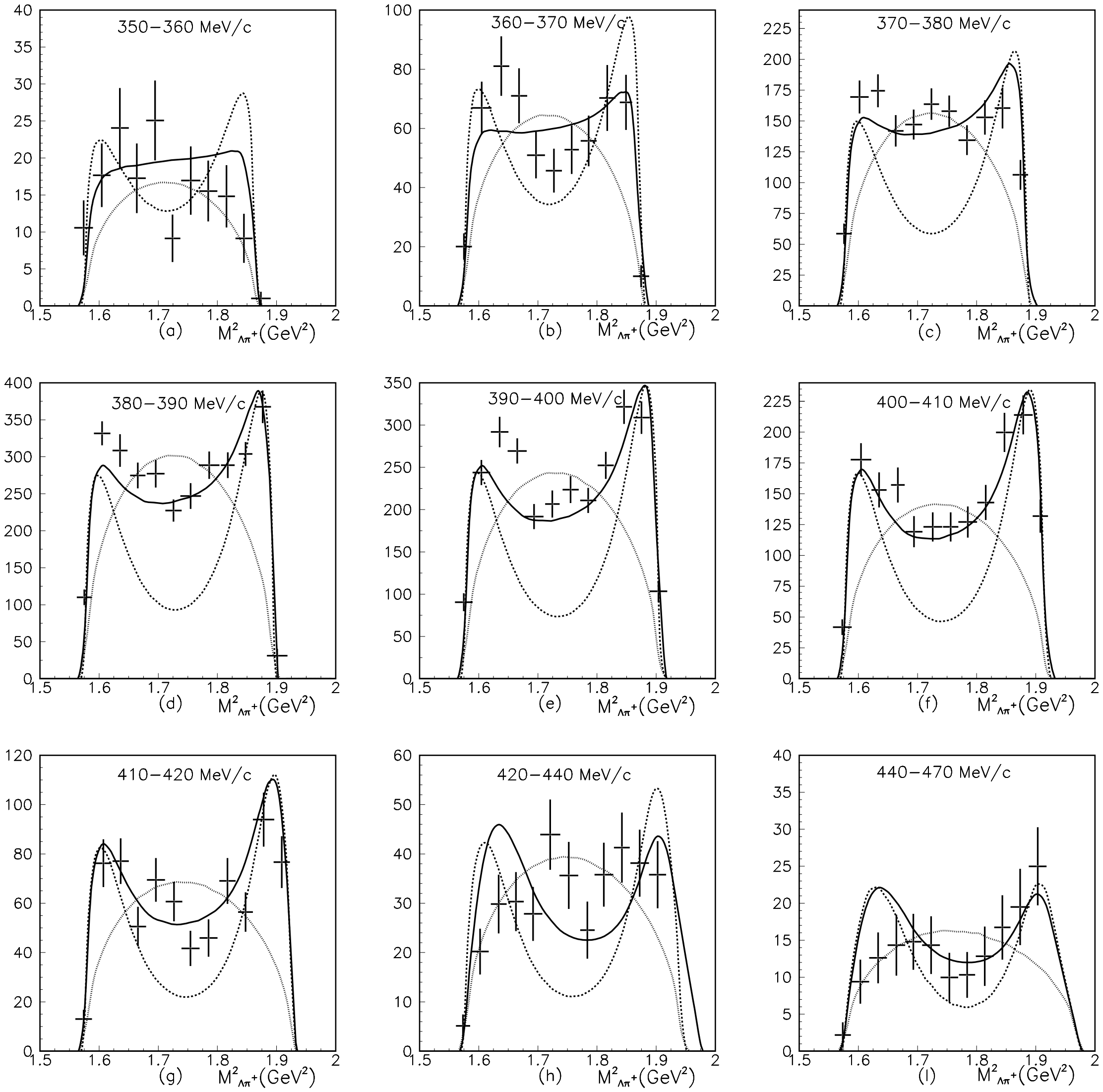

FIG. 5: Theoretical $\Lambda\pi^+$ invariant mass squared distribution for various K^- beam momenta compared with data [11]. The dotted line is for the pure $\Sigma^*(1385)$ with $J^P = \frac{3}{2}^+$; the solid line includes $\Sigma^*_{1/2}$ in addition with $R_{3/2} = 0.60$.

In summary, we study the $K^-p \to \Lambda\pi^-\pi^+$ reaction at $Plab_{(K^-)} = 0.25 - 0.60$ GeV. In our calculations we take into account all possible form factors and final state interactions. We find that by including 40% $\Sigma^*_{1/2}$ contribution the theory agrees much better with the experimental data [11] for $Plab_{(K^-)}$ in the range of $0.355 - 0.42$ GeV, corresponding to the Kp center-of-mass energies just under the $\Lambda^*(1520)$ peak. Through the analysis, the difference between the two cases, with or without $\Sigma^*_{1/2}$, comes from the different partial waves, namely,

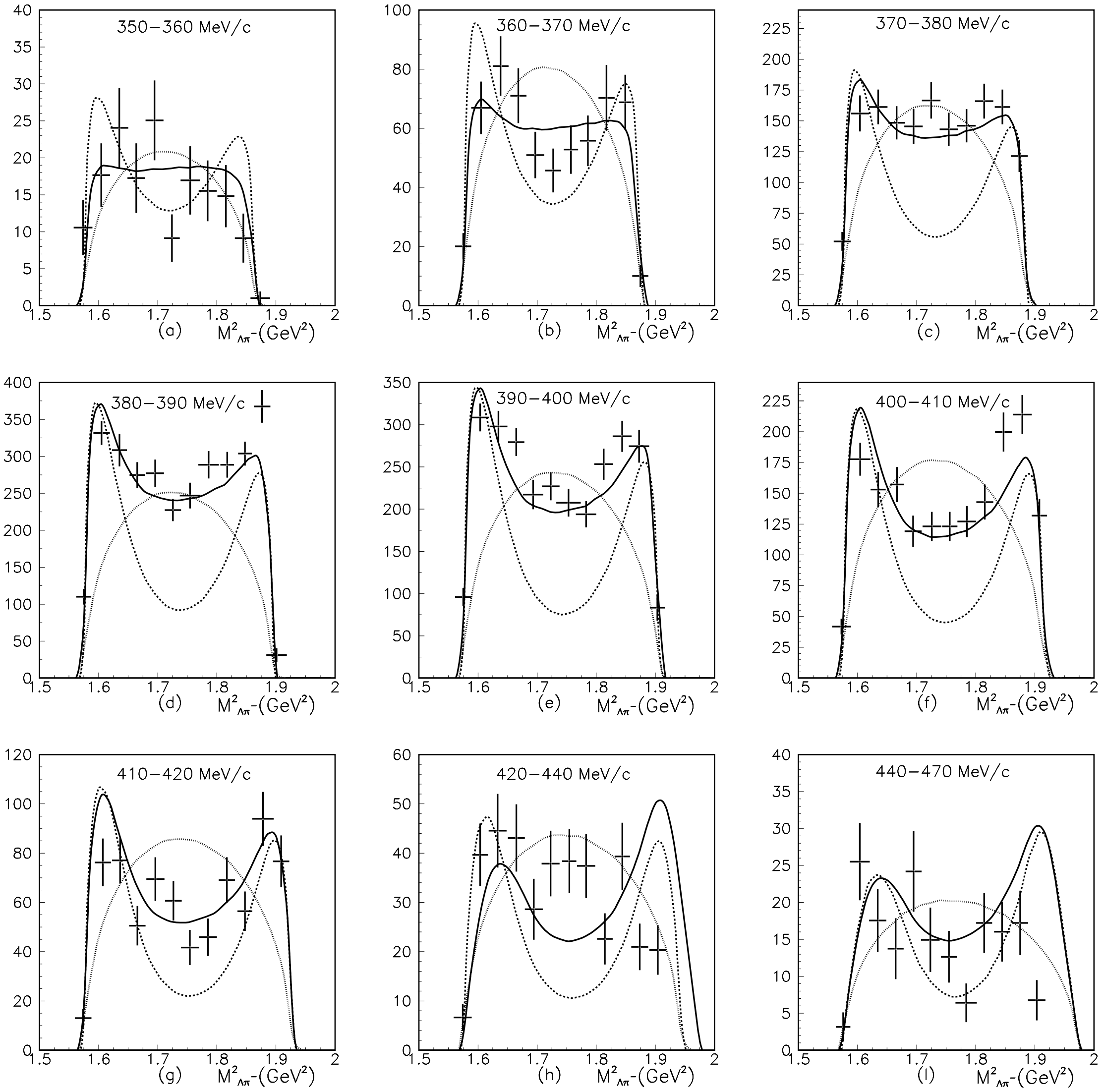

FIG. 6: Theoretical $\Lambda\pi^-$ invariant mass squared distribution for various K^- beam momenta compared with data [11]. The dotted line is for the pure $\Sigma^*(1385)$ with $J^P = \frac{3}{2}^+$; the solid line includes $\Sigma^*_{1/2}$ in addition with $R_{3/2} = 0.60$.

S-wave of $\Sigma^*_{3/2}\pi$ verus P-wave of $\Sigma^*_{1/2}\pi$ from $\Lambda^*(1520)$ decays, and the different width of the two particles. The results of this work strongly suggest that the new particle Σ^* with $J^P = \frac{1}{2}^-$ exists in the $\Lambda^*(1520) \to \Sigma^*\pi \to \Lambda\pi\pi$ decays. Higher statistic data experiments are necessary to establish this new resonance and to understand its property.

Acknowledgements We thank Pu-ze Gao for useful discussions. This work is partly supported by the National Natural Science Foundation of China (NSFC) under grants Nos.

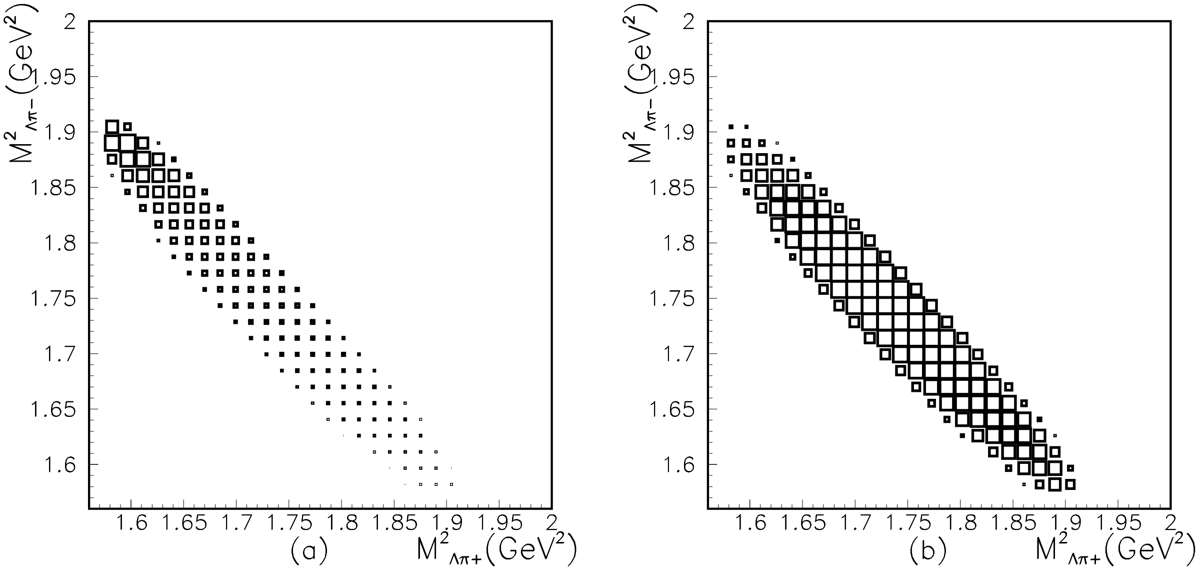

FIG. 7: Dalitz plots (a) and (b) corresponding to the reactions $K^-p \rightarrow \Lambda^* \rightarrow \Sigma^{*-}_{3/2}\pi^+ \rightarrow \Lambda\pi^+\pi^-$ and $K^-p \rightarrow \Lambda^* \rightarrow \Sigma^{*-}_{1/2}\pi^+ \rightarrow \Lambda\pi^+\pi^-$, respectively, at $Plab_{(K^-)} = 0.394$ GeV.

10875133, 10821063, 10635080, 10665001, and by the Chinese Academy of Sciences under project No. KJCX3-SYW-N2, and by the Ministry of Science and Technology of China (2009CB825200).

---

[1] C. Amsler *et al.* [Particle Data Group], Phys. Lett. B **667** (2008) 1.

[2] G.T.Garvey, J.C.Peng, Prog. Part. Nucl. Phys. **47**, (2001) 203, and references therein.

[3] C. Helminen and D. O. Riska, Nucl. Phys. A **699**, 624 (2002) [arXiv:nucl-th/0011071].

[4] A. Zhang, Y. R. Liu, P. Z. Huang, W. Z. Deng, X. L. Chen and S. L. Zhu, High Energy Phys. Nucl. Phys. **29**, 250 (2005) [arXiv:hep-ph/0403210].

[5] B. S. Zou, Eur. Phys. J. A **35**, 325 (2008) [arXiv:0711.4860 [nucl-th]].

[6] D. Jido, J. A. Oller, E. Oset, A. Ramos and U. G. Meissner, Nucl. Phys. A **725**, 181 (2003) [arXiv:nucl-th/0303062].

[7] B. S. Zou, Int. J. Mod. Phys. A **21**, 5552 (2006).

[8] D. Asner *et al.*, Int. J. Mod. A**24**, 1.[arXiv:0809.1869[hep-ex]].

[9] J. J. Wu, S. Dulat and B. S. Zou, Phys. Rev. D **80**, 017503 (2009) arXiv:0906.3950 [hep-ph].

[10] L. Roca, S. Sarkar, V. K. Magas and E. Oset, Phys. Rev. C **73**, 045208 (2006) [arXiv:hep-ph/0603222].

[11] T. S. Mast, M. Alston-Garnjost, R. O. Bangerter, A. Barbaro-Galtieri, F. T. Solmitz and R. D. Tripp, Phys. Rev. D **7**, 5 (1973).

[12] Z. Ouyang, J.J.Xie, B.S. Zou and H.S. Xu, Int. J. Mod. Phys. E **18**, 281 (2009). [arXiv:nucl-th/09021818]

[13] Y. Oh, C. M. Ko and K. Nakayama, Phys. Rev. C **77**, 045204 (2008) [arXiv:0712.4285 [nucl-th]].

[14] A. Reuber, K. Holinde and J. Speth, Czech. J. Phys. **42**, 1115 (1992).

[15] B. S. Zou and D. V. Bugg, Eur. Phys. J. A **16**, 537 (2003) [arXiv:hep-ph/0211457].

[16] M. B. Watson, M. Ferro-Luzzi and R. D. Tripp, Phys. Rev. **131**, 2248 (1963).

[17] R. Armenteros *et al.*, Nucl. Phys. B **21**, 15 (1970).